Applied Catalysis A: General 471 (2014) 1–11

Contents lists available at ScienceDirect

Applied Catalysis A: General

journal homepage: www.elsevier.com/locate/apcata

# Hafnium salts of dodeca-tungstophosphoric acid catalysts for liquid phase benzylation of anisole with dibenzylether

Chowdari Ramesh Kumar[a,b], N. Rambabu[a], N. Lingaiah[b,*], P.S. Sai Prasad[b], A.K. Dalai[a,*]

[a] Department of Chemical and Biological Engineering, University of Saskatchewan, Saskatoon, SK, S7N 5A9, Canada
[b] Catalysis Laboratory, I&PC Division, CSIR-Indian Institute of Chemical Technology, Hyderabad 500007, AP, India

ARTICLE INFO

*Article history:*
Received 21 June 2013
Received in revised form 29 October 2013
Accepted 1 November 2013
Available online 1 December 2013

*Keywords:*
Anisole
Benzylation
Dibenzylether
Hafnium
Heteropoly tungstate
Keggin ion

ABSTRACT

A series of hafnium salts of heteropoly tungstate ($Hf_xTPA$) catalysts were prepared by exchanging the counter cations (hydrogen) of heteropoly tungstate with hafnium ions. The prepared catalysts were characterized by FT-IR, Laser Raman, temperature programmed desorption of ammonia, scanning electron microscopy, and X-ray photo electron spectroscopy. FT-IR and Raman characterization results suggested retention of the Keggin ion structure of heteropoly acid. Pyridine adsorbed FT-IR spectra of the catalysts showed that generation of Lewis acidic sites was due to the presence of hafnium ions in the catalyst. Activity of these catalysts was investigated for liquid phase benzylation of anisole with dibenzylether. In the partial exchanged catalyst ($Hf_{0.5}TPA$), higher conversion was due to high mobility of residual protons. The catalytic activity of $Hf_xTPA$ depended on the exchangeable hafnium ions in the secondary structure of heteropoly tungstate that, in turn, relates to variation in acidity of the catalyst. Thermal stability and structural properties of the $Hf_{0.5}TPA$ catalyst were studied by treating it at different temperatures. Dibenzylether conversion and selectivity towards benzylated products were found to depend on the anisole to dibenzylether ratio, reaction temperature, and catalyst loading.



## 1. Introduction

Over the past two decades polyoxometalates (POMs) have received increasing interest in the area of catalysis [1,2] because of their participation in important industrial processes related for the materials [3], nanotechnology [4], biology [5,6], supramolecular materials [7,8], and colloidal science [9]. POMs are made up of oxygen and early transition metals of groups V and VI in their highest oxidation states, such as V, Nb, Ta, Mo, W [10]. Depending on the structural type, POMs are broadly classified into two types; (i) isopolyoxometalates and (ii) heteropolyoxometalates. Isopolyoxometalate is a metal oxide framework with only $d^0$ metal cations, such as $W^{6+}$, $Mo^{5+}$ [11]. Heteropolyoxometalates are composed of a metal-oxide framework along with a hetero atom in the form of anion (e.g., $PO_4^{3-}$, $SO_4^{2-}$). There are many structures proposed for heteropolyoxometalates in which Keggin type and Wells–Dawson structures are well studied.

The Keggin type of heteropoly anion is generally represented as $[XM_{12}O_{40}]^{x-}$, where *X* is the hetero atom, such as P, Si, Al, or Ge in tetrahedral fashion, and M is the addenda atom, usually $W^{6+}$ or $Mo^{6+}$. The Keggin ion is made of an assembly of twelve $MO_6$ octahedrons sharing their corners or edges with a central $XO_4$ tetrahedron. Hydrogen forms of these heteropolyoxometalates are called heteropoly acids (HPAs), for example, $H_3[PW_{12}O_{40}]$, $H_4[SiW_{12}O_{40}]$, and $H_3[PMo_{12}O_{40}]$. Among the Keggin type heteropoly acids, W-based heteropoly acids are relatively more acidic compared to other heteropoly acids [12]. Misono et al. [13,14] reported the primary, secondary, and tertiary hierarchical structures for HPAs to understand their heterogeneous catalysis. Accordingly, the heteropoly anion is a primary structure; the regular arrangement of the polyanions, counter cations, and additional molecules in three-dimension is called a secondary structure; and the assembly of this structure into solid particles is known as a tertiary structure, which relates to their properties such as particle size, surface area, and pore structure [15].

HPAs are widely used as catalysts in a number of homogeneous and heterogeneous acid–base and redox type catalytic reactions, due to their specific physicochemical properties such as high acidity and oxidizing properties [16–18]. The redox properties of heteropoly acids can be tuned in a systematic way by substituting the metal into primary and secondary structures [14,19–21]. Generally, heteropoly acids are highly soluble in polar solvents. HPAs can be made heterogeneous by supporting them on suitable supports [22–24] and/or substitution of counter ions ($H^+$) with metal ions [25–29]. Metal exchanged HPAs can be classified into two groups: group A are the HPAs in which protons are exchanged with small metal ions like $Na^+$, $Al^{3+}$, or $Cu^{2+}$; and group B are those HPAs

* Corresponding authors. Tel.: +1 306 966 4771; fax: +1 306 966 4777.
*E-mail addresses:* nakkalingaiah@iict.res.in (N. Lingaiah), ajay.dalai@usask.ca (A.K. Dalai).

0926-860X/$ – see front matter © 2013 Published by Elsevier B.V.
http://dx.doi.org/10.1016/j.apcata.2013.11.001

containing large metal ions like $Cs^+$, $Sn^{2+}$, or $Sn^{4+}$ [25,30]. Substitution of certain metal ions generates Lewis acidic sites in heteropoly acids, in which metal ions act as electron pair acceptors [25].

Friedel–Crafts alkylation (FCA) of aromatic compounds is an important process in petroleum, chemical, and pharmaceutical industries [31,32]. Conventionally, diarylmethane and substituted diarylmethane derivates produced by the reaction of aromatics with benzyl chloride produce HCl that causes corrosion and is environmentally hazardous. Use of benzyl alcohol or dibenzylether as a benzylating agent instead of benzyl halides, produces water as a by-product, which is non-hazardous [33,34]. Shimizu et al. [25,26] reported that the polyvalent-metal salts of dodecatungstophosphate ($Cs^+$, $Ag^+$, $Y^{3+}$, $Fe^{3+}$, $Bi^{3+}$, $Ru^{3+}$, $Al^{3+}$, $Ti^{4+}$, $Zr^{4+}$, $Ti^{4+}$, $Hf^{4+}$, and $Sn^{4+}$) act as effective heterogeneous catalysts for Friedel–Crafts acylation and alkylation of aromatics with carboxylic acids and alcohols, respectively. Metal salts of heteropoly acid for hydrolysis of cellobiose and cellulose are also reported in the literature [35]. However, the literature shows few reports on detailed characterization of metal salts of dodeca-tungstophosphoric acid. The application of simple hafnium salts is an emerging area in organic synthesis [36–42]. Shiina et al. studied FCA of aromatic nucleophiles with intermediary benzyl silyl ethers using $HfCl_4$ as Lewis acid [36]. Zhang et al. have developed $HfCl_4/HfO_2$ catalyst for arylation of benzyl alcohols [42]. This system catalyzes the reaction of dichloromethane with benzene to yield diphenylmethane with high selectivity. However, most of these catalysts have limitation to reuse. In our previous reports, modification of tungstophosphoric acid with metal ions such as $Sn^{2+}$, $Sm^{3+}$ and $Al^{3+}$ was reported [27,28,33]. Since $HfCl_4$ is Lewis acid, it can be used to modify the heteropoly acids with $Hf^{4+}$ to generate Lewis acidic sites. To the best of our knowledge, no detailed study has been reported on hafnium salts of tungstophosphoric acid for organic synthesis.

The objective of the present study was to prepare hafnium salts of tungstophosphoric acid catalysts with varying hafnium content and to characterize them by FT-IR, Laser Raman, $NH_3$-TPD, X-ray photoelectron spectroscopy, pyridine FT-IR, and SEM. The catalytic activity of the prepared catalysts was investigated by benzylation of anisole with dibenzylether, and changes in the surface and structural properties of the catalysts with calcination temperature were studied using different characterization techniques. The effects of reaction temperature, catalyst weight, and anisole to dibenzylether molar ratio were also studied to optimize the reaction conditions.

## 2. Experimental

### 2.1. Materials and chemicals

The following analytical grade chemicals were used for catalyst preparation and benzylation of anisole reaction. 12-tungstophosphoric acid (Sigma-Aldrich), hafnium chloride (Sigma-Aldrich), benzyl alcohol (EM Science), dibenzylether (Alfa-Aesar), 4-methoxydiphenylmethane (Matrix Scientific, Columbia), anisole (Alfa-Aesar). Ammonia balanced with helium, hydrogen, air, and nitrogen gases were procured from Praxair Canada.

### 2.2. Preparation of hafnium salt of tungstophosphoric acid

The hafnium-exchanged 12-tungstophosphoric acid ($Hf_x$TPA) catalyst series was prepared according to the procedure previously reported in the literature [26]. The catalysts were prepared as follows: required amount of TPA was dissolved in distilled water, and to this solution, the calculated amount of $HfCl_4$ dissolved in distilled water was added with continuous stirring, forming a white precipitate. The resultant mixture was stirred for 2 h and the excess water was evaporated on a rotary evaporator. The dried catalyst was kept in a hot air oven for further drying and finally calcined at 300 °C for 2 h. The catalyst was denoted as $Hf_x$TPA, where $x$ represents the number of hafnium ions, which varied from 0.25 to 0.75.

### 2.3. Characterization of catalysts

The FT-IR spectra were recorded on a PerkinElmer spectrum 100 series (USA) infrared spectrometer using the KBr pellet method in the wave number range of 4000–400 $cm^{-1}$, with a resolution of 4 $cm^{-1}$ at room temperature. The nature of the acid sites (Bronsted and Lewis) of the catalysts was determined with chemisorbed pyridine. The pyridine adsorption studies were carried out in the diffuse reflectance infrared Fourier transform (DRIFT) mode. Prior to the pyridine adsorption catalysts were degassed under vacuum at 200 °C for 3 h followed by suspending dry pyridine. Then, the excess pyridine was removed by heating the sample at 120 °C for 1 h. After cooling the sample to room temperature, FT-IR spectra of the pyridine-adsorbed samples were recorded. The Bronsted and Lewis acid sites intensity ratios were calculated from the intensities of the corresponding absorbance values.

The ratio of Bronsted and Lewis acidities was estimated from the IR peak intensity corresponding to these acid sites.

Confocal micro-Raman spectra were recorded at room temperature in the range of 200–1200 $cm^{-1}$ using a Renishaw Invia Reflex Raman microscope equipped with an $Ar^+$ laser (Spectra-Physics model 127) operating at an excitation wavelength of 514.5 nm and an 1800 line/mm grating. The laser was focused onto the powdered sample using a 5× objective, giving a spot size of approximately 1 μm. The laser power was 1.8 mW measured at the sample. The instrument's calibration was verified with a Si(1 1 0) sample that was measured at 520 $cm^{-1}$.

The acidity of the catalysts was measured by temperature programmed desorption of ammonia (TPD–$NH_3$). In a typical experiment, 0.1 g of catalyst was loaded and pre-treated in a helium atmosphere at 300 °C for 2 h. After pre-treatment, the temperature was brought to 100 °C and the adsorption of $NH_3$ was carried out by passing a mixture of 10% $NH_3$ on He over the catalyst for 1 h. The catalyst surface was then flushed with He at 100 °C for 2 h to flush off the physisorbed $NH_3$. TPD of $NH_3$ was carried with a temperature ramp of 10 °C/min and the desorbed ammonia was monitored using a thermal conductivity detector (TCD) of a gas chromatograph.

X-ray photo electron spectroscopy (XPS) measurements were conducted on a KRATOS AXIS 165 with a DUAL anode (Mg and Al) apparatus using Mg $K_\alpha$ anode. The non-monochromatized Al $K_\alpha$ X-ray source ($h\nu$ = 1486.6 eV) was operated at 12.5 kV and 16 mA. Before analysis, each sample was out-gassed for about 3 h at 100 °C under vacuum of $1.0 \times 10^{-7}$ T to minimize surface contamination. The XPS instrument was calibrated using Au as standard. For energy calibration, the carbon 1s photoelectron line was used. The carbon 1s binding energy was taken as 285 eV. Charge neutralization of 2 eV was used to balance the charge up of the sample. The spectra were deconvoluted using Sun Solaris Vision-2 curve resolver. The location and full width at half maximum (FWHM) value for the species were first determined using the spectrum of a pure sample. Symmetric Gaussian shapes were used in all cases. Binding energies for identical samples were, in general, reproducible within ±0.1 eV.

Scanning electron microscope images (SEM) were obtained using a JEOL 6010LV instrument to observe the morphology of the prepared samples.

### 2.4. Alkylation reaction procedure

The alkylation reactions were carried out in a 50 ml two-necked round bottom flask with a reflux condenser with nitrogen inlet for

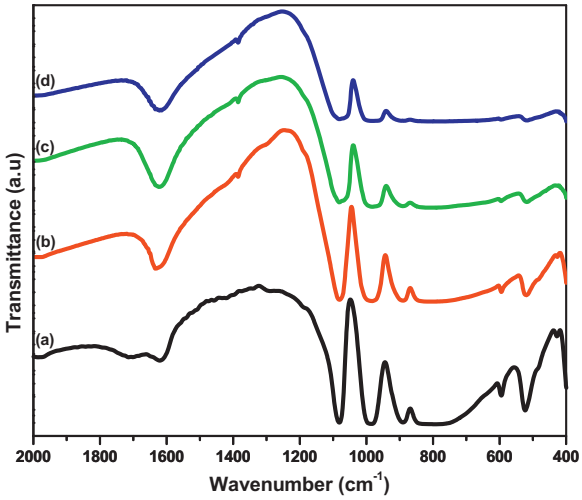


**Fig. 1.** FT-IR of (a) TPA, (b) $Hf_{0.25}$TPA, (c) $Hf_{0.5}$TPA, and (d) $Hf_{0.75}$TPA.

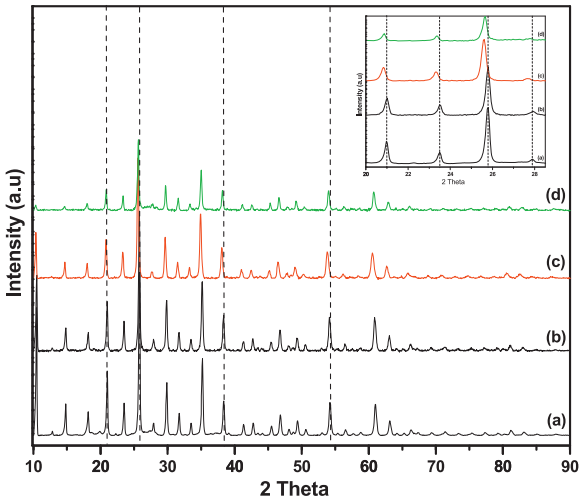


**Fig. 2.** X-ray diffraction patterns of (a) TPA, (b) $Hf_{0.25}$TPA, (c) $Hf_{0.5}$TPA, and (d) $Hf_{0.75}$TPA.

nitrogen purging into the reaction mixture and a septum for sample removal. In a typical run, 10 g of anisole and 3.08 g of dibenzyl ether along with 0.1 g catalyst were taken into a flask. The reaction was carried out at temperature of 120 °C.

The reaction mixture was withdrawn at different intervals and analyzed by gas chromatography equipped with a stibil wax column and flame ionization detector. The reaction products were identified using GC–MS and also confirmed by using retention times of standard samples.

## 3. Results and discussion

### 3.1. FT-IR spectroscopy

Fig. 1 shows the FT-IR spectra of hafnium salts of 12-tungstophosphoric acid along with the parent acid. Pure TPA (Fig. 1(a)) shows characteristic bands in the fingerprint region, at 1081, 988, 896, and 796 $cm^{-1}$ that indicate P–O, W=$O_t$ ($O_t$—refers to the terminal oxygen), W–$O_c$–W ($O_c$—refers to the corner oxygen), and W–$O_e$–W ($O_e$—refers to edge sharing oxygen), respectively [28]. Apart from these four bands, two more bands observed at 596 and 524 $cm^{-1}$ are related to bending vibrations of P–O and W–O, respectively. All these characteristic bands of TPA are present in hafnium salts of TPA, indicating the retention of Keggin ions after exchange of the counter ions with hafnium ions. The band at 1630 $cm^{-1}$ is assigned to the H–O–H bending vibration mode [43].

### 3.2. X-ray diffraction patterns

Fig. 2 shows the X-ray diffraction patterns of $Hf_x$TPA catalysts. TPA shows the characteristic peaks of the Keggin ion at 2$\theta$ of 10.5°, 18.3°, 23.7°, 26.1°, 30.2°, 35.6°, and 38.8°. The characteristic peaks of TPA were observed in all the catalysts. As reported in the literature, when TPA protons were exchanged with metal ions such as $Cs^+$ and $Sm^{3+}$ the XRD peaks corresponding to TPA were shifted to lower angles, indicating the expansion of unit cell volume [28,44]. Similarly, it was noticed that with Hf content increased from 0.25 to 0.75, the relative intensity of characteristic peaks related to the Keggin ion decreased and shifted to lower angles, which indicates that expansion of the unit cell volume as the size of the $Hf^{4+}$ is much greater than that of proton. The shift in XRD peaks is clearly observed in the inset of the Fig. 2, which indicates an exchange of $Hf^{4+}$ ions for the protons of TPA. This was further supported by FT–IR results.

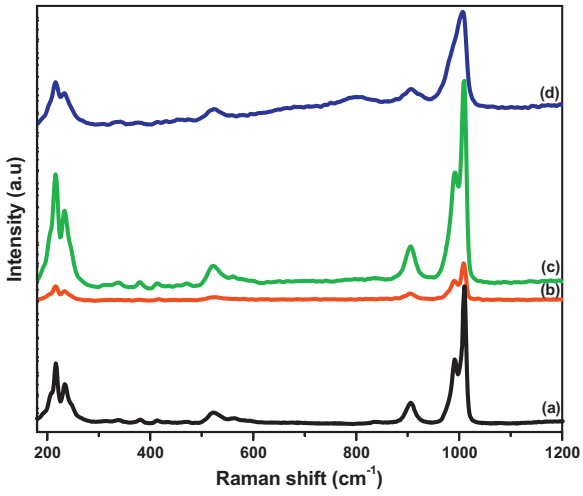


**Fig. 3.** Raman spectra of (a) TPA, (b) $Hf_{0.25}$TPA, (c) $Hf_{0.5}$TPA, and (d) $Hf_{0.75}$TPA.

### 3.3. Raman spectra

The existence of the Keggin ion was further confirmed by Laser Raman spectroscopy. This is an effective technique to determine the presence of different metal oxides and molecular structure of the immobilized samples because it is more sensitive to the Keggin unit. Fig. 3 shows the Laser Raman spectra of the parent 12-tungstophosphoric acid and hafnium salts of TPA. Pure crystalline TPA (Fig. 3 (a)) showed peaks at 1006, 990, 900, 535, 231, and 215 $cm^{-1}$ [45–47]. Hafnium salt of heteropoly tungstate (Fig. 3(b–d)) also showed the characteristic peaks of the parent acid. The bands at 1006 and 990 $cm^{-1}$ are characteristic peaks of asymmetric and symmetric vibrations of W=$O_t$ (t-terminal). These bands are unresolved in the $Hf_{0.75}$TPA sample (Fig. 3 (d)) that showed only one band at 1006 $cm^{-1}$. The Raman bands at 900 and 535 are ascribed to asymmetric stretching vibrations of W–$O_c$–W ($O_c$-corner sharing bridging oxygen atom) and symmetric stretching vibrations of W–$O_e$–W ($O_e$-edge sharing bridging oxygen atom), respectively. The peak observed at 231 $cm^{-1}$ is related to W-O-W bending mode of vibration, and the peak observed at 215 $cm^{-1}$ might be due to the coupling between two bending modes of vibrations [45]. Hafnium salts of tungstophosphoric acid show all the characteristic bands related to the Keggin ion,

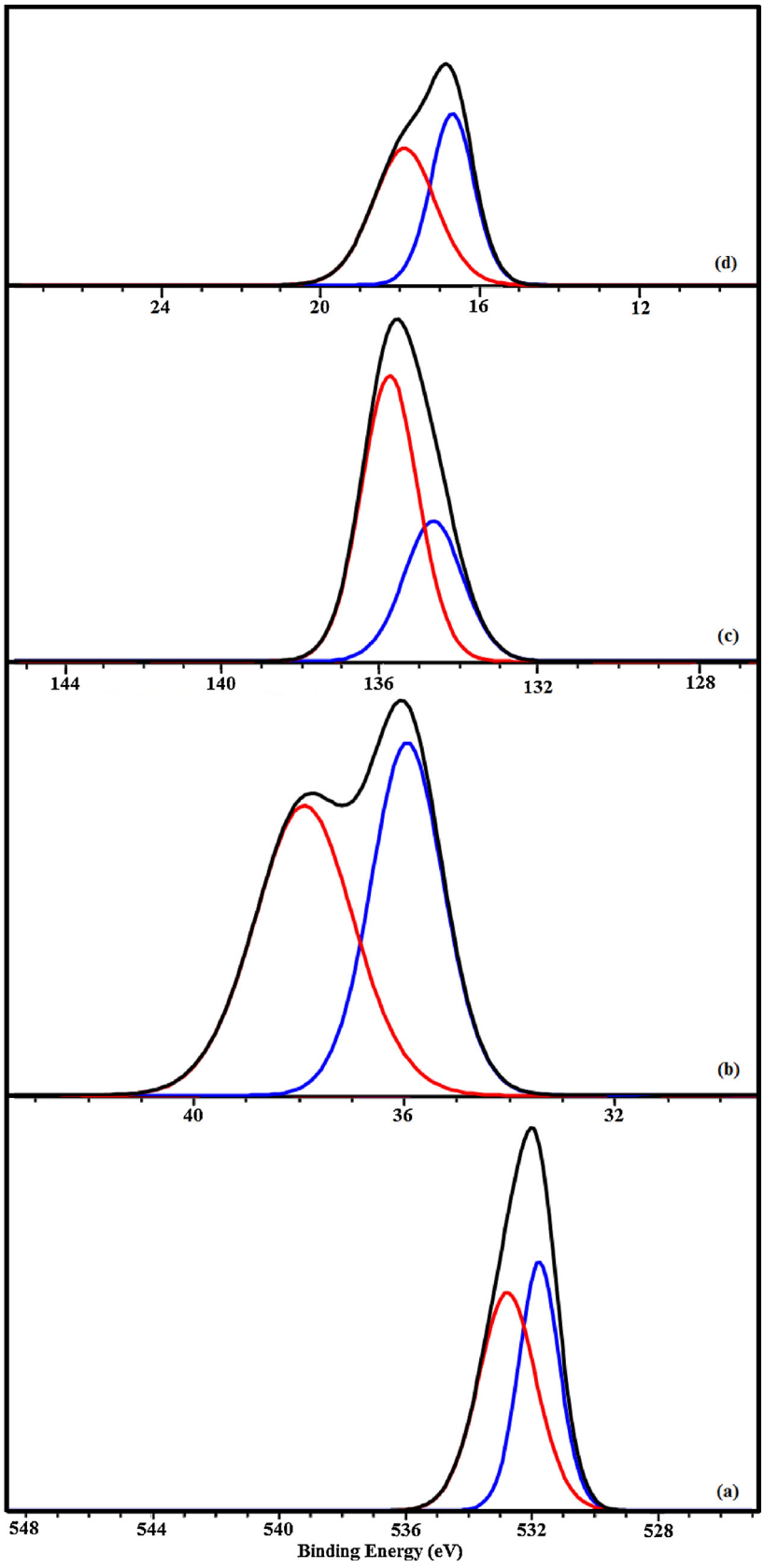


**Fig. 4.** X-ray photo electron spectroscopy of $Hf_{0.5}$TPA (a) O 1s, (b) W 4f, (c) P 2p, and (d) Hf 4f.

**Table 1**
Binding energy values of $Hf_{0.5}TPA$ catalyst.

| Element | Binding energy (eV) |
|---|---|
| Hf (4f) | 16.681<br>(46.2%)17.905 (53.8%) |
| P (2p) | 134.695<br>(33.9%)135.763 (66.1%) |
| W (4f) | 35.940<br>(47.1%)37.910 (52.9%) |
| O (1s) | 531.779<br>(44.2%)532.776 (55.8%) |

confirming the existence of the primary structure of heteropoly tungstate.

### 3.4. X-ray photo electron spectroscopy

X-ray photoelectron spectroscopy (XPS) is a versatile surface analysis technique that can be used for compositional, chemical, and electronic states of elements. XPS spectra of O 1s, W 4f, P 2p, and Hf 4f of the $Hf_{0.5}TPA$ catalyst are shown in Fig. 4 and binding energy values are summarized in Table 1. Fig. 4(a) shows the XPS spectra of O 1s in the binding energy region of 531.8 and 532.8 eV as a doublet. The peak at 531.8 eV is attributed to oxygen present in the W–O–W, and the second peak at 532.8 eV is ascribed to W–O–P [28]. XPS of W 4f deconvoluted into two peaks in the range of 35.9–37.9 eV (Fig. 4(b)). Binding energies of 35.9 and 37.9 eV correspond to W $4f_{7/2}$ and W $4f_{5/2}$, respectively that are typical binding energy values of $W^{6+}$ oxidation state [28,33].

XPS spectra of P 2p, two peaks are observed with 1.1 eV separation owing to spin–orbit coupling (see Fig. 4(c)). The binding energy values of P 2p (Table 1) confirm the presence of phosphorus in the form of phosphate [46]. Binding energies of Hf 4f were observed at 16.7 ($4f_{7/2}$) and 17.9 eV ($4f_{5/2}$), which correspond to the Hf–O bond. This suggests that Hf is combined onto the oxygen atom of the heteropoly anion to form the Hf–O bond and confirms the presence of $Hf^{4+}$ state.

### 3.5. Pyridine adsorbed FT-IR spectra

Pyridine FT-IR analysis was used to investigate the presence of Bronsted and Lewis acidic sites in the catalyst. The pyridine-adsorbed FT-IR spectra show various features in the region of 1400–1600 $cm^{-1}$ due to the stretching vibrations of M–N (metal–nitrogen) and N–H (pyridinium ion). The band assigned to the pyridinium ion is recorded at 1536 $cm^{-1}$ and the one at 1449 $cm^{-1}$ is associated to pyridine adsorbed onto Lewis-type acid sites. Pyridine FT–IR of $Hf_xTPA$ samples were recorded at room temperature and the results are shown in Fig. 5. Hafnium salt of heteropoly tungstate catalysts contains both Bronsted and Lewis acidic sites, as evidenced by bands at $\overline{\upsilon} = 1533$ and 1440 $cm^{-1}$, respectively [27,28]. The Bronsted and Lewis acid sites intensity ratios were calculated from the intensities of absorbance at 1533 and 1440 $cm^{-1}$.The presented in Table 2. From this Table it can be noticed that the Bronsted to Lewis acidity intensity ratio decreased with an increase in the Hf content. The band at $\overline{\upsilon} = 1485$ $cm^{-1}$ corresponds to the combined band that originated from pyridine adsorbed on Bronsted and Lewis acidic sites. Lewis acidity arises due to the exchange of protons of TPA with hafnium ions. With an increase in the hafnium content from 0.25 to 0.75 (Fig. 5(a–c), respectively), intensity of the band associated with Lewis acidic sites increased and those corresponding to Bronsted acidic sites were decreased. Since the Bronsted to Lewis acidity intensity ratio

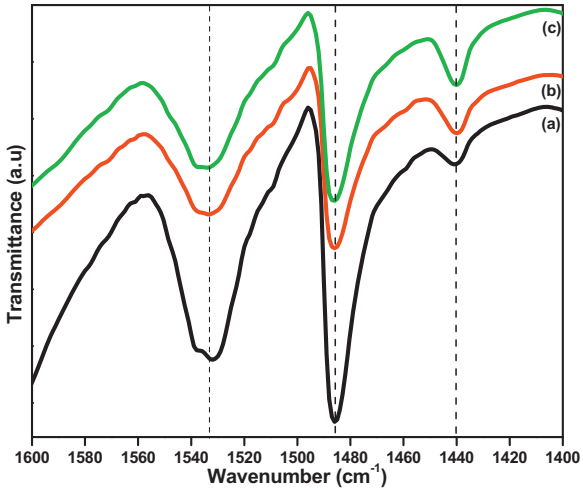


**Fig. 5.** Pyridine adsorbed FT-IR spectra of (a) Hf0.25TPA, (b) $Hf_{0.5}TPA$, and (c) $Hf_{0.75}TPA$.

also decreased with an increase in the Hf content, these results confirm that Lewis acidity was generated by the exchange of TPA protons with $Hf^{4+}$.

### 3.6. Temperature programmed desorption of ammonia

Acidity of the hafnium salts of heteropoly tungstate catalysts was measured by temperature programmed desorption of ammonia. The desorbed ammonia from the catalyst surface was calculated and acid strength distribution values are presented in the Table 3. Fig. 6 shows the TPD of ammonia profiles, in which two desorption peaks are observed for all samples. The low temperature desorption peak at 150 °C might be due to the ammonia molecules adsorbed on Lewis acidic sites and the high temperature desorption peak at 570 °C might be due to the ammonia molecules adsorbed on Bronsted acidic sites. When ammonia is adsorbed on heteropoly acid, generally ammonium salt of heteropoly acid is formed and desorption of ammonia occurs at higher temperatures [48]. Fig. 6(a–c) shows that with an increase in the Hf content, the desorption peak at higher temperatures was shifted to lower temperatures. The intensity of the peak at higher temperatures decreased with an increase in Hf content, whereas, at lower temperatures the intensity of the desorption peak increased. These results suggest that with an increase in hafnium content from 0.25

**Table 2**
Bronsted to Lewis acid sites intensity ratio of $Hf_xTPA$ catalysts.

| S. no. | Catalyst | $B/L$ ratio ($I_{1533}/I_{1440}$) |
|---|---|---|
| 1. | $Hf_{0.25}TPA$ | 1.56 |
| 2. | $Hf_{0.5}TPA$ | 1.17 |
| 3. | $Hf_{0.75}TPA$ | 1.16 |

**Table 3**
Acid strength distribution of $Hf_xTPA$ catalysts.

| Catalyst | Acidity (mmol/g) | | |
|---|---|---|---|
| | Weak/moderate | Strong | Total acidity |
| $Hf_{0.25}TPA$ | 0.036 | 0.621 | 0.657 |
| $Hf_{0.5}TPA$ | 0.138 | 0.516 | 0.654 |
| $Hf_{0.75}TPA$ | 0.298 | 0.257 | 0.555 |
| 400-$Hf_{0.5}TPA$ | 0.128 | 0.369 | 0.497 |
| 500-$Hf_{0.5}TPA$ | 0.022 | 0.032 | 0.054 |
| 600-$Hf_{0.5}TPA$ | 0.025 | 0.005 | 0.030 |
| 750-$Hf_{0.5}TPA$ | 0.031 | 0.012 | 0.043 |

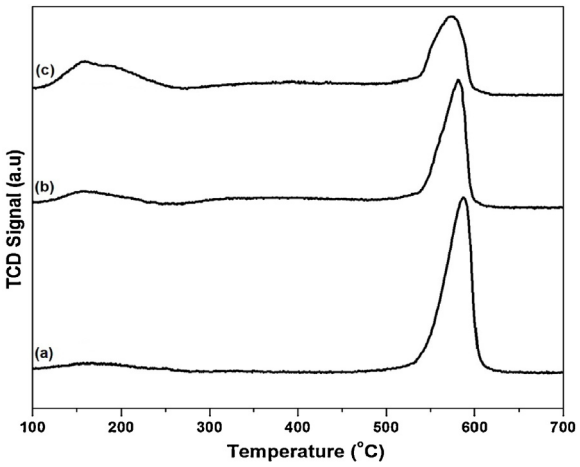


**Fig. 6.** Ammonia TPD of (a) $Hf_{0.25}$TPA, (b) $Hf_{0.5}$TPA, and (c) $Hf_{0.75}$TPA.

to 0.75, Lewis acidity is increased. For the $Hf_{0.25}$TPA sample, a weak desorption peak is observed in the region of 120–280 °C due to low hafnium content, whereas, the $Hf_{0.75}$TPA sample showed a strong desorption peak in the same region (120–280 °C). The intensity of the desorption peak at higher temperatures is decreased, indicating the presence of more Lewis acidic sites in the $Hf_{0.75}$TPA catalyst. The desorbed ammonia values related to weak/moderate acidic sites also increased with an increase in Hf content (Table 3). The partial exchanged catalysts $Hf_{0.25}$TPA and $Hf_{0.5}$TPA exhibited high acidity compared to $Hf_{0.75}$TPA catalyst.

FT-IR of pyridine adsorbed spectra results are also in good agreement with these results. The partial exchanged catalyst ($Hf_{0.5}$TPA) showed moderate acidic sites related to Lewis acid, which resulted in high mobility of the residual protons [27].

### 3.7. SEM analysis

Structural morphology of $Hf_x$TPA catalysts were studied by scanning electron microscopy (Fig. 7). Hafnium salts of heteropoly tungstate particles are irregular, not uniform, and agglomerated. The $Hf_{0.5}$TPA sample appears to have small particles compared to the other two samples.

### 3.8. Evaluation of catalytic activity for benzylation of anisole with dibenzylether

Fig. 8 shows the conversion of dibenzylether and product distribution for benzylation of anisole with dibenzylether over $Hf_x$TPA catalysts along with the parent TPA. The main products in benzylation of anisole are *p*-benzyl anisole and *o*-benzyl anisole. As shown in Fig. 8, TPA showed only 35% of dibenzylether conversion with selectivity toward desired products i.e., *p*- and *o*- are 47 and 41 (mol%), respectively. In the case of the $Hf_x$TPA catalyst, activity of dibenzylether conversion increased from 68% to 97%, when the *x* value increased from 0.25 to 0.5, and when hafnium content was further increased to 0.75, the conversion of dibenzylether decreased to 84%. In the case of the $Hf_{0.25}$TPA catalyst, 68% of dibenzylether conversion was observed, selectivity towards *p*- and *o*- were 53% and 45%, respectively. A by-product (benzyl alcohol) was also found with a selectivity of 2%. The $Hf_{0.75}$TPA catalyst showed 84% of dibenzylether with 51:48 (*p*-:*o*-) selectivity. The $Hf_{0.5}$TPA catalyst showed much higher conversion of dibenzylether (97%) and achieved a *p*-:*o*- selectivity of 52:48, without formation of benzyl alcohol, even though the total acidity of the $Hf_{0.25}$TPA catalyst was same as the $Hf_{0.5}$TPA catalyst (Table 3). The higher conversion of dibenzylether in the case of $Hf_{0.5}$TPA may be due to high mobility of residual protons. $Hf_{0.5}$TPA possesses both Lewis and Bronsted acidic sites, as evidenced by pyridine FT-IR spectra (Fig. 5). Acidity results of TPD of ammonia (Fig. 6) are also in good agreement with the observed catalytic activity. A plausible mechanism is proposed and presented in Scheme 1, in which Bronsted and Lewis acid sites are involved in the reaction. Path I and II shows the adsorption of dibenzylether molecule on the Bronsted and Lewis acidic sites respectively, available on the catalyst surface. In the second step attack of anisole molecule on adsorbed dibenzylether molecule leads to cleavage of dibenzylether molecule and produces benzylated products (*o*- and *p*-). In the next step reaction between another anisole molecule and adsorbed benzyl alcohol (produced due to cleavage of dibenzylether) produces benzylated products or adsorbed benzyl alcohol which is produced due to cleavage of dibenzylether may desorbed form the catalyst surface produces benzyl alcohol as a by-product in the reaction mixture.

#### 3.8.1. Effect of catalyst calcination temperature

$Hf_{0.5}$TPA was the most active catalyst and subjected to calcination at different temperatures to investigate the surface-structural properties, thermal stability, and its influence on benzylation of anisole with dibenzylether. Fig. 9 shows the effect of catalyst calcination temperature on benzylation of anisole with dibenzylether. Conversion of dibenzylether was decreased with an increase in calcination temperature. The catalyst was calcined at a temperature of 300 °C and showed maximum conversion of dibenzylether with 97% yield of benzylated products. When the catalyst was calcined at 400 and 500 °C, conversion of dibenzylether was 84% and 1%, respectively. To better understand the variations in catalytic activity of the catalysts with calcination temperature, they were further characterized by FT-IR, Laser Raman, and TPD of ammonia.

Fig. 10 shows the FT-IR spectra of $Hf_{0.5}$TPA catalyst calcined at different temperatures. The IR bands related to the Keggin ion are clearly observed in the catalysts calcined at 300 and 400 °C, indicating that the Keggin ion structure can be retained up to a calcination temperature of 400 °C (Fig. 10(a and b)). It was noticed that a slight decrease in the intensity of the peaks related to Keggin ion, for the catalyst calcined at 400 °C compared to catalyst calcined at 300 °C. This might be due to partial degradation of the Keggin ion of $Hf_{0.5}$TPA catalyst. Decomposition of the Keggin ion

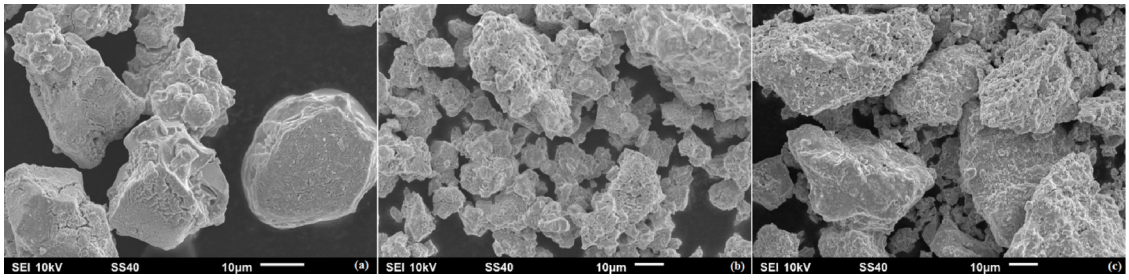


**Fig. 7.** SEM images of (a) $Hf_{0.25}$TPA, (b) $Hf_{0.5}$TPA, and (c) $Hf_{0.75}$TPA.

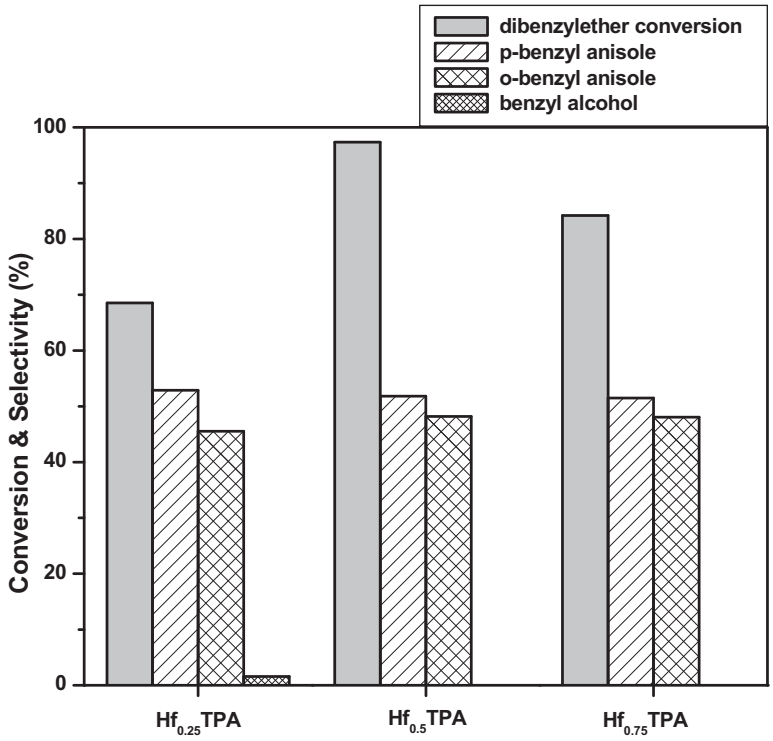


**Fig. 8.** Catalytic activity of the $Hf_xTPA$ (where $x = 0.25$, 0.5, and 0.75) catalysts for benzylation of anisole with dibenzylether. *Reaction conditions*: Reaction temperature 120 °C, catalyst calcination temperature 300 °C, catalyst loading 100 mg, Anisole to dibenzylether molar ratio 12:2 and reaction time 1 h.

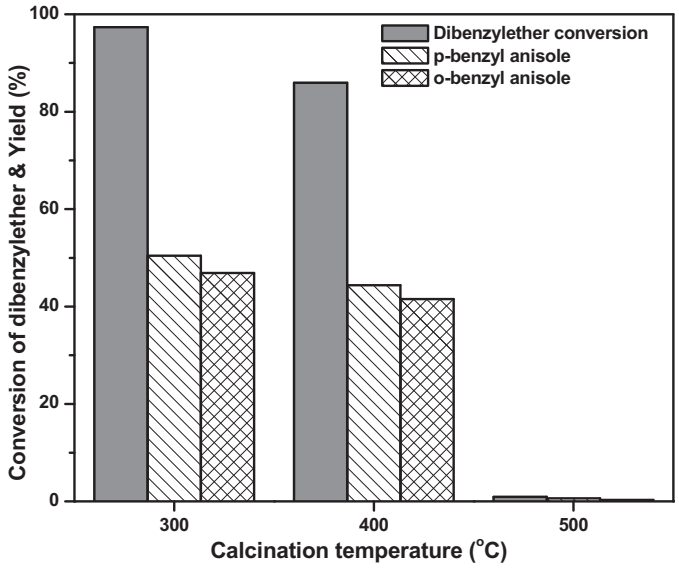


**Fig. 9.** Effect of $Hf_{0.5}TPA$ catalyst calcination temperature on benzylation of anisole with dibenzylether. *Reaction conditions*: Reaction temperature 120 °C, catalyst loading 100 mg, anisole to dibenzylether molar ratio 12:2 and reaction time 1 h.

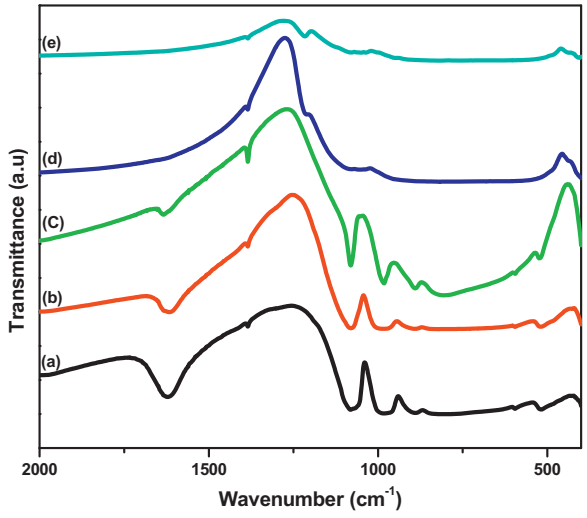


**Fig. 10.** FT-IR spectra of $Hf_{0.5}TPA$ catalyst calcined at (a) 300 °C, (b) 400 °C, (c) 500 °C, (d) 600 °C, and (e) 750 °C.

started at 500 °C, as it shows sharp IR bands related to the Keggin ion (Fig. 10(c)). A further increase in calcination temperature (600 and 750 °C) resulted in complete decomposition of the Keggin ion of heteropoly tungstate into constituent metal oxide $WO_3$ [23].

Fig. 11 shows the Laser Raman spectra of the $Hf_{0.5}TPA$ catalyst calcined at different temperatures in the range of 300–750 °C. The catalysts calcined at 300 °C (Fig. 11(a)) clearly shows that bands at 1006 and 990 $cm^{-1}$ are associated with asymmetric and symmetric vibrations of $W{=}O_t$ ($O_t$—terminal oxygen). Catalyst calcined at 400 °C also showed these peaks related to Keggin ion with low intensity, which indicates the partial degradation of Keggin ion. These results are in good agreement with the results obtained from FT-IR spectra. The catalyst calcined at 500 °C (Fig. 11(c)) also shows a weak band at 1006 $cm^{-1}$ related to asymmetric vibrations of $W{=}O_t$, as well as strong bands at 790, 690, and 272 $cm^{-1}$. The Raman bands at 790 and 690 $cm^{-1}$ are ascribed to stretching vibrations of W–O–W and the band at 272 $cm^{-1}$ relates to the characteristic bending mode vibration of $WO_3$ [49]. With an increase in calcination temperature of the catalyst from 600 to 750 °C (Fig. 11(d and e)), the band related only to $WO_3$ phase was observed. These results suggest that the catalyst is thermally stable upto 400 °C and that a further increase in temperature causes decomposition of the Keggin ion of heteropoly tungstate.

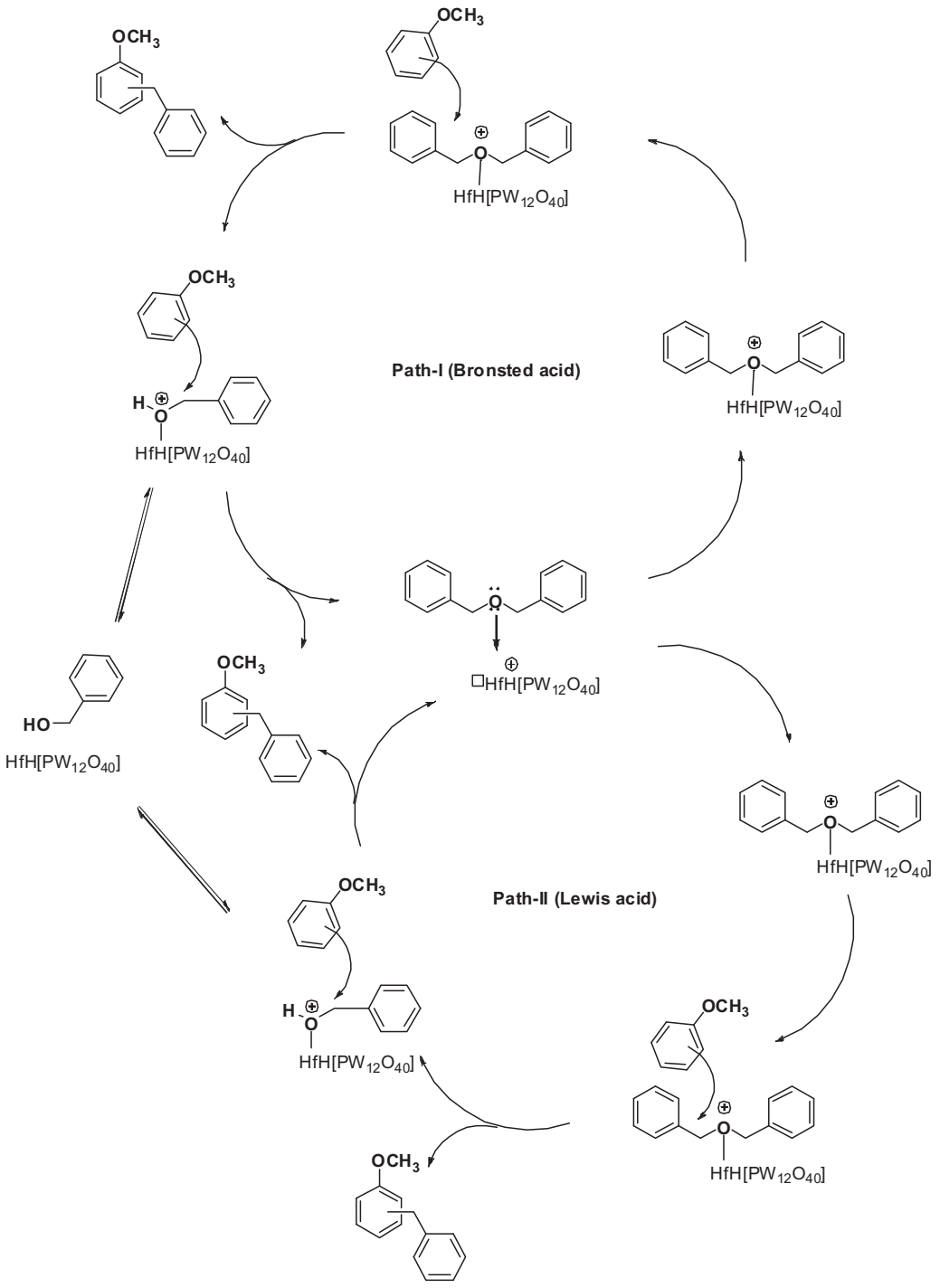


**Scheme 1.** Plausible mechanism for benzylation of anisole with dibenzylether.

Acidity of the catalysts calcined at different temperatures was analyzed by $NH_3$-TPD (Fig. 12). The catalyst calcined at 300 °C (Fig. 12(a)) showed a strong desorption peak centered at 620 °C. The catalyst calcined at 400 and 500 °C (Fig. 12(b and c)) showed a small desorption peak at higher temperatures (580 °C) that were absent for the catalysts calcined at higher temperatures of 600 and 750 °C (Fig. 12(d and e)), indicating no considerable acidity for these catalysts compared to the catalyst calcined at lower temperatures of 300 and 400 °C. This might be due to the decomposition of heteropoly anion at higher calcination temperature. The catalyst calcined at 400 °C showed characteristic peaks of Keggin ion in the FT–IR and Raman spectra with low intensity compared to catalyst calcined at 300 °C. However, in TPD of ammonia pattern of catalyst calcined at 400 °C a shift in high temperature desorption peak to higher temperature (700 °C) was observed. This might be due to partial degradation of the Keggin units of $Hf_{0.5}$TPA this may be accountable for the benzylation activity.

The experimental result of catalytic activity for benzylation of anisole indicates that catalytic activity depends on the acidity of catalysts, which in turn is related to the existence of the heteropoly anion. To optimize the dibenzylether conversion, the effect of reaction parameters such as reaction temperature, catalyst weight, and anisole to dibenzylether molar ratio were also studied.

**Table 4**
Effect of catalyst weight.

| Catalyst weight (mg) | Conversion of dibenzyl ether (%) | Selectivity (%) | | |
|---|---|---|---|---|
| | | *o*- | *p*- | Benzyl alcohol |
| 50 | 47.0 | 40.5 | 47.0 | 12.5 |
| 100 | 64.0 | 46.0 | 50.7 | 3.3 |
| 150 | 89.60 | 48.0 | 52.0 | – |
| 200 | 100.0 | 47.0 | 53.0 | – |

*Reaction conditions*: Reaction temperature 120 °C, catalyst calcination temperature 300 °C, anisole to dibenzylether molar ratio 12:2 and reaction time 30 min.

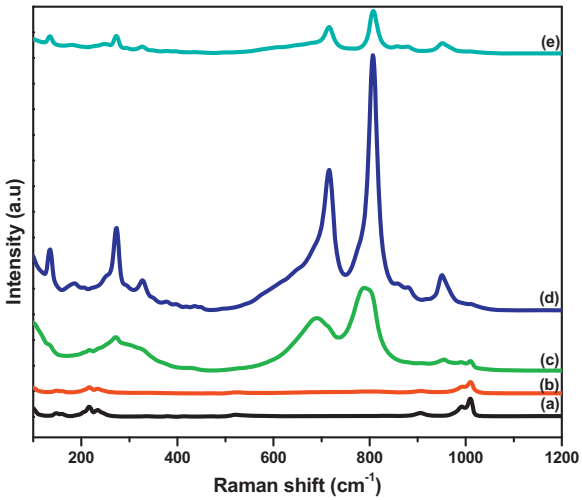


**Fig. 11.** Raman spectra of $Hf_{0.5}$TPA catalyst calcined at (a) 300 °C, (b) 400 °C, (c) 500 °C, (d) 600 °C, and (e) 750 °C.

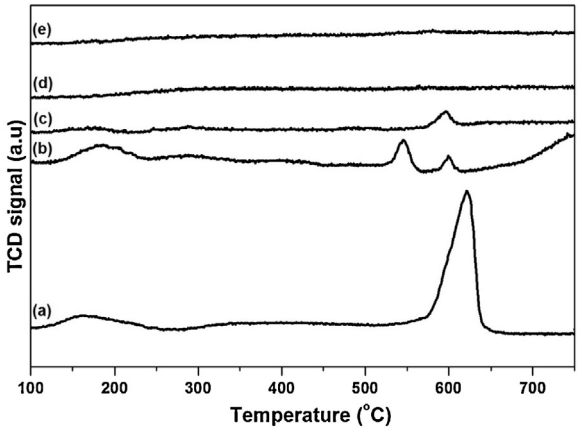


**Fig. 12.** Ammonia TPD of $Hf_{0.5}$TPA calcined at (a) 300 °C, (b) 400 °C, (c) 500 °C, (d) 600 °C, and (e) 750 °C.

### 3.8.2. Optimization of reaction parameters

*3.8.2.1. Effect reaction temperature.* Benzylation of anisole with dibenzylether was carried out at various temperatures ranging from 80 to 140 °C at a reaction time of 15 min (Fig. 13). There was no significant conversion of dibenzylether at 80 °C (not shown). An increase in reaction temperature from 80 to 140 °C increased the dibenzylether conversion and complete conversion without any by-products at 140 °C. A by-product benzyl alcohol was observed when the reaction was carried out at lower temperatures. Selectivity towards benzylated products increased with an increase in reaction temperature.

*3.8.2.2. Effect of catalyst weight.* The effect of catalyst weight on dibenzylether conversion was studied by varying the catalyst amount from 50 to 200 mg. Experimental results are shown in Table 4 at a reaction time of 30 min. An increase in catalyst weight from 50 to 200 mg increased the conversion of dibenzylether. A by-product was observed when a lower amount (50 and 100 mg) of catalyst was used, but when 200 mg of catalyst was used, a complete conversion of dibenzylether with selectivity of *p*- to *o*- of 53 and 47%, respectively, was observed without any by-product.

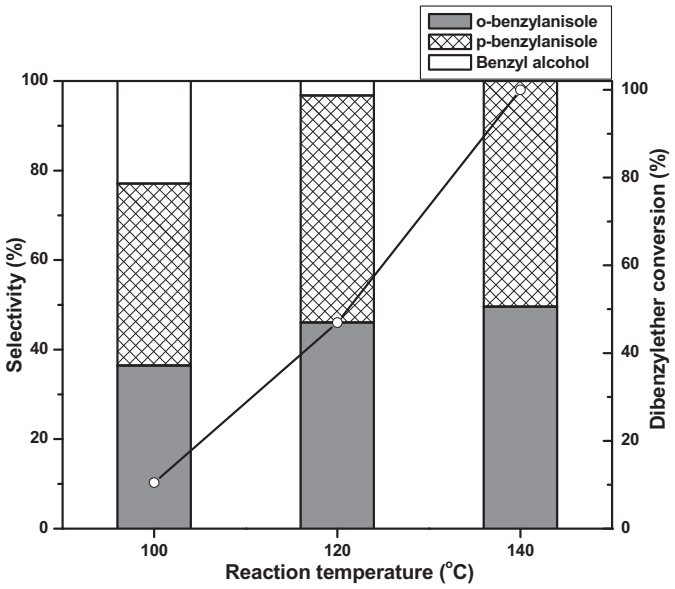


**Fig. 13.** Effect of reaction temperature on benzylation of anisole with dibenzylether. *Reaction conditions*: Anisole to dibenzylether molar ratio 12:2, catalyst ($Hf_{0.5}$TPA) loading 100 mg and reaction time 15 min.

*3.8.2.3. Effect of molar ratio.* To assess its effect on catalytic activity and product selectivity over the $Hf_{0.5}$TPA catalyst, benzylation of anisole with dibenzylether was carried out by varying the molar ratio of anisole to dibenzylether from 12:1 to 12:4 (Table 5). With an increase in reactant molar ratio from 12:1 to 12:4, the conversion of dibenzylether decreased. The higher concentration of dibenzylether leads to a higher adsorption of dibenzylether molecules onto the catalyst surface, and less availability of anisole molecules retards the benzylation reaction. In all the cases, there was no marginal change in product selectivity and maximum conversion (100%) of dibenzylether was observed in the 12:1 molar ratio.

**Table 5**
Influence of anisole to dibenzylether molar ratio.

| Anisole to DBE molar ratio | Conversion of DBE (%) | Selectivity (%) | |
|---|---|---|---|
| | | *o*- | *p*- |
| 12:1 | 100 | 47.0 | 53.0 |
| 12:2 | 85.16 | 47.7 | 52.3 |
| 12:4 | 75.81 | 48.2 | 51.8 |

*Reaction conditions*: Reaction temperature 120 °C, Catalyst calcination temperature 300 °C, catalyst loading 100 mg and reaction time 30 min.

**Table 6**
Comparison of the catalytic activity of $Hf_{0.5}$TPA catalyst with other reported acid catalysts for benzylation of aromatics with dibenzylether.

| Catalyst | Substrate | Reaction temperature (°C) | Reaction time (h) | Conversion of dibenzylether (%) | Product yield (%) | Ref. |
|---|---|---|---|---|---|---|
| $Hf_{0.5}$TPA | Anisole | 140 | 0.25 | 100 | 100 | Present study |
| HPW(50)/MCM-41 | Benzene | 90 | 1.67 | 50 | | [50] |
| Sulfated zirconia/MCM-41 | Benzene | 180 | 24 | 100 | 95* | [51] |
| Ir/Sn bimetallic catalyst | Anisole | 90 | 0.5 | | 99 | [34] |
| $FeCl_3$ | Benzene | 90 | 12 | | 68 | [52] |

* Diphenylmethane selectivity.

### 3.9. Comparison of the catalytic activity of $Hf_{0.5}$TPA with reported catalysts

The benzylation of aromatics with benzyl alcohol reaction was studied well, but few reports are available on the benzylation of aromatics with dibenzylether. In the present study, the catalytic activity of optimized catalyst $Hf_{0.5}$TPA was compared with those of reported catalysts for the benzylation of aromatics with dibenzylether (DBE) and the results are shown in Table 6. The $Hf_{0.5}$TPA catalyst exhibited a complete conversion of DBE within 0.25 h with 100% selectivity towards benzylated products when compared to other catalysts. Kamalakar et al. studied the role of dibenzylether (DBE) in benzylation of benzene at a reaction temperature of 90 °C. The time required for 50% conversion of DBE was about 1.67 h. Al-Hazmi et al. examined the benzylation of benzene with DBE. The conversion of DBE was 100% and selectivity of the product (diphenylmethane) was 95%. However, 100% conversion of DBE was achieved only at high reaction time (24 h) and temperature (180 °C). Ir/Sn bimetallic catalyst was reported by Podder et al. for benzylation of arenes with ethers. The benzylation of anisole reaction was studied at 90 °C and the selectivity of benzylated product was 99% within 0.5 h. But the main disadvantage of this catalyst is limitation to reuse. Wang et al. investigated the benzylation of benzene with DBE over $FeCl_3$ catalyst. The obtained desired product diphenylmethane yield was only 68% after 12 h of reaction time. However, this catalyst is well known traditional homogeneous Lewis acid catalyst and it cannot be recycled. This study indicates that the $Hf_{0.5}$TPA catalyst is highly active and selective for benzylation reaction with DBE compared to above reported catalysts.

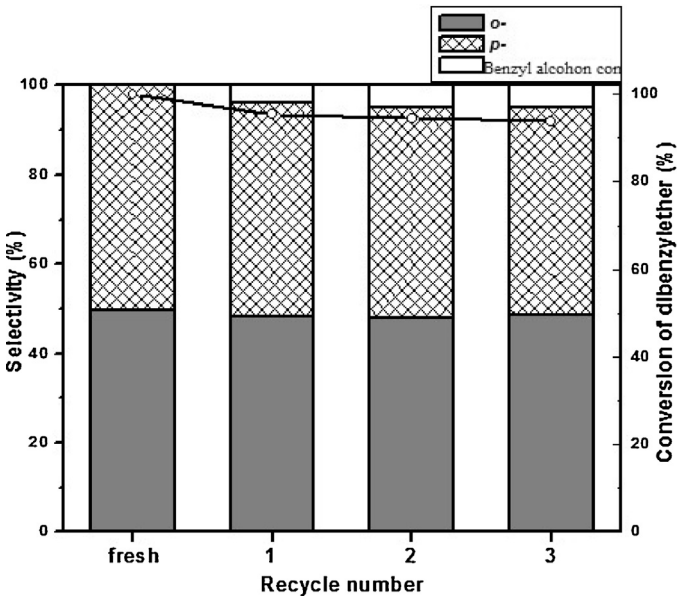


**Fig. 14.** Reusability study of $Hf_{0.5}$TPA catalyst.

### 3.10. Catalyst reusability

To determine the efficiency of the $Hf_{0.5}$TPA catalyst, reusability experiments were carried out. After completion of the reaction, the catalyst was separated from the reaction mixture by centrifugation, followed by ethyl acetate washes. The catalyst was then dried in a hot air oven at 120 °C for 1 h and reused for benzylation of anisole with dibenzylether. Catalytic activity of the reused catalyst is presented in Fig. 14. The recycling results showed that there is marginal change in the selectivity of the benzylated products. However, formation of the by-product (benzyl alcohol) was observed when the catalyst was reused. The selectivity of benzyl alcohol was only 5% after the third recycle run of the catalyst. It was found that, the catalytic activity of the catalyst decreased by ~6% after the fourth run when compared to the first run with a fresh catalyst. It is concluded that the $Hf_{0.5}$TPA catalyst can be reused for benzylation reaction without any considerable loss in the activity.

## 4. Conclusions

Hafnium salt of heteropoly tungstate catalysts was prepared with retention of the Keggin ion structure by varying hafnium content. Catalytic activity depends on exchangeable hafnium ions with protons of TPA. Partial exchange of TPA protons with $Hf^{4+}$ ions results in high mobility of residual protons and exhibits high activity and selectivity towards benzylated products compared to parent TPA, due to the presence of both Lewis and Bronsted acidic sites. A plausible mechanism, involving Bronsted and Lewis acidic sites in the reaction is also proposed for benzylation of anisole with dibenzylether. The optimized reaction conditions for benzylation of anisole with dibenzylether are: Catalyst calcination temperature 300 °C, 100 mg catalyst loading, 140 °C reaction temperature and 12:2 molar ratio of anisole to dibenzylether.

## Acknowledgments

Ramesh Kumar acknowledges the University of Saskatchewan and the Canadian Bureau for International Education (CBIE) for financial assistance through the Canadian Commonwealth scholarship program. Support from the Canada Research Chair (CRC) program is also acknowledged.

## References

[1] R. Neumann, A.M. Khenkin, I. Vigdergauz, Chem. Eur. J. 6 (2000) 875–882.
[2] N. Mizuno, K. Yamaguchi, K. Kamata, Coord. Chem. Rev. 249 (2005) 1944–1956.
[3] M.I. Khan, J. Solid State Chem. 152 (2000) 105–112.
[4] D.L. Long, L. Cronin, Chem. Eur. J. 12 (2006) 3698–3706.
[5] B. Hasenknopf, Front. Biosci. 10 (2005) 275–287.
[6] K. Nomiya, H. Torii, T. Hasegawa, Y. Nemoto, K. Nomura, K. Hashino, M. Uchida, Y. Kato, K. Shimizu, M. Oda, J. Inorg. Biochem. 86 (2001) 657–667.
[7] D. Volkmer, B. Bredenkotter, J. Tellenbroker, P. Kogerler, D.G. Kurth, P. Lehmann, H. Schnablegger, D. Schwahn, M. Piepenbrink, B. Krebs, J. Am. Chem. Soc. 124 (2002) 10489–10496.
[8] S.Q. Liu, D. Volkmer, D.G. Kurth, J. Cluster Sci. 14 (2003) 405–419.
[9] T.B. Liu, E. Diemann, H.L. Li, A.W.M. Dress, A. Muller, Nature 426 (2003) 59–62.
[10] M.T. Pope, A. Muller, Angew. Chem. Int. Ed. 30 (1991) 34–48.

[11] J.T. Rhule, C.L. Hill, D.A. Judd, Chem. Rev. 98 (1998) 327–358.
[12] T. Okuhara, N. Mizuno, M. Misono, Adv. Catal. 41 (1996) 113–252.
[13] M. Misono, K. Sakata, Y. Yoneda, W.Y. Lee, Proceedings Seventh International Congress on Catalysis, Tokyo, 1980, p. 1047.
[14] M. Misono, Chem. Commun. (2001) 1141–1152.
[15] M. Misono, Proceedings 10th International Congress on Catalysis, Budapest, 1992, Elsevier /Akademiai Kiado, Amsterdam/Budapest, 1993, p. 69.
[16] C.L. Hill, C.M. Prosser-McCartha, Coord. Chem. Rev. 143 (1995) 407–455.
[17] I.V. Kozhevnikov, Chem. Rev. 98 (1998) 171–198.
[18] M. Misono, Catal. Rev. Sci. Eng. 29 (1987) 269–321.
[19] I.V. Kozhevnikov, Catal. Rev. Sci. Eng. 37 (1995) 311–352.
[20] I.K. Song, M.A. Barteau, Korean J. Chem. Eng. 19 (2002) 567–573.
[21] M.H. Youn, D.R. Park, J.C. Jung, H. Kim, M.A. Barteau, I.K. Song, Korean J. Chem. Eng. (2007) 51–54.
[22] G.S. Armatas, G. Bilis, M. Louloudi, J. Mater. Chem. 21 (2011) 2997–3005.
[23] Ch. Ramesh Kumar, P.S. Sai Prasad, N. Lingaiah, Appl. Catal., A 384 (2010) 101–106.
[24] L. Xu, W. Li, J. Hu, X. Yang, Y. Guo, Appl. Catal., B 90 (2009) 587–594.
[25] K. Shimizu, K. Niimi, A. Satsuma, Appl. Catal., A 349 (2008) 1–5.
[26] K. Shimizu, K. Niimi, A. Satsuma, Catal. Commun. 9 (2008) 980–983.
[27] Ch.R. Kumar, K.T. Venkateswara Rao, P.S. Sai Prasad, N. Lingaiah, J. Mol. Catal. A: Chem. 337 (2011) 17–24.
[28] Ch.R. Kumar, K. Jagadeeswaraiah, P.S. Sai Prasad, N. Lingaiah, Chem. Cat. Chem. 4 (2012) 1360–1367.
[29] H. Firouzabadi, N. Iranpoor, F. Nowrouzi, Tetrahedron 60 (2004) 10843–10850.
[30] H. Niiyama, Y. Saito, E. Echigoya, Proceedings Seventh International Congress on Catalysis, Tokyo, 1980, p. 1416.
[31] G.A. Olah, Friedel-Crafts and Related Reactions Part I, 2, Wiley-Interscience, New York, 1964.
[32] T.W. Bastock, J.H. Clark, Speciality Chemicals, Elsevier, London, 1991.
[33] Ch.R. Kumar, P.S. Sai Prasad, N. Lingaiah, J. Mol. Catal. A: Chem. 350 (2011) 83–90.
[34] S. Podder, S. Roy, Tetrahedron 63 (2007) 9146–9152.
[35] K. Shimizu, H. Furukawa, N. Kobayashi, Y. Itaya, A. Satsuma, Green Chem. 11 (2009) 1627–1632.
[36] I. Shiina, M. Suzuki, K. Yokoyama, Tetrahedron Lett. 43 (2002) 6395–6398.
[37] X.H. Hao, A. Yoshida, J. Nishikido, Tetrahedron Lett. 46 (2005) 2697–2700.
[38] N. Asao, T. Shimada, T. Shimada, J. Am. Chem. Soc. 123 (2001) 10899–10902.
[39] K. Ishihara, S. Ohara, H. Yamamoto, Science 290 (2000) 1140–1142.
[40] Y. Hayashi, M. Nakamura, S. Nakao, Angew. Chem. Int. Ed. 41 (2002) 4079–4082.
[41] N. Asao, H. Tomeba, Y. Yamamoto, Tetrahedron Lett. 46 (2005) 27–30.
[42] C.Y. Zhang, X.Q. Gao, J.H. Zhang, X.J. Peng, Chin. Chem. Lett. 20 (2009) 913–916.
[43] M. Hashimoto, G. Koyano, N. Mizuno, J. Phys. Chem. B 108 (2004) 12368–12374.
[44] A. Corma, A. Martinez, C. Martinez, J. Catal. 164 (1996) 422–432.
[45] T. Takashima, R. Nakamura, K. Hshimoto, J. Phys. Chem. C 113 (2009) 17247–17253.
[46] K. Mohan Reddy, N. Seshu Babu, P.S. Sai Prasad, N. Lingaiah, Catal. Commun. 9 (2008) 2525–2531.
[47] E. Caliman, J.A. Dias, S.L.C. Dias, F.A.C. Garcia, J.L. Macedo, L.S. Almeida, Microporous Mesoporous Mater. 132 (2010) 103–111.
[48] J.K. Kim, J.H. Choi, J.H. Song, J. Yi, I.K. Song, Catal. Commun. 27 (2012) 5–8.
[49] S. Songara, V. Gupta, M.K. Patra, J. Singh, L. Saini, G.S. Gowd, S.R. Vadera, N. Kumar, J. Phys. Chem. Solids 73 (2012) 851–857.
[50] G. Kamalakar, K. Komura, Y. Kubota, Y. Sugi, J. Chem. Technol. Biotechnol. 81 (2006) 981–988.
[51] M.H. Al-Hazmi, A.W. Apblett, Catal. Sci. Technol. 1 (2011) 621–630.
[52] B.Q. Wang, S.K. Xiang, Z.P. Sun, B.T. Guan, P. Hu, K.Q. Zhao, Z.J. Shi, Tetrahedron Lett. 49 (2008) 4310–4312.